Frequency conversion in two-dimensional photonic structure

Babic, L.

Chapter 2

Second harmonic generation in gallium phosphide nanowires

2.1 Introduction

Semiconductor nanowires are essentially one-dimensional (1D) nanostructures that have subwavelength lateral dimensions and typical lengths of several micrometers. Since the introduction of nanowires by Yazawa et al. [35], many advances have been made in tuning their electrical and optical properties by controlling their growth. Today, nanowires represent a class of metamaterials that shows promise for many device applications compatible with on-chip technologies. The list of nanowire-based optoelectronic devices includes lasers [14–16], waveguides [17, 18], photodetectors [19–21], solar cells [22, 23], nonlinear optical converters [24, 25], biological and chemical sensors [26].

The high length-to-width aspect ratios of the nanowires combined with the high refractive index of semiconductors can lead to strong polarization anisotropy that facilitates some of their applications. Wang et al. [19] were the first to experimentally demonstrate the optical anisotropy of a single indium phosphide (InP) nanowire by measuring its photoluminescence (PL) properties. The authors point out the possibility of using InP nanowires as polarization sensitive photodetectors incorporated into photonic-based circuits.

Recent advances in the bottom-up fabrication method of metal-organic vapor phase epitaxy (MOVPE) [13], made it possible to grow a high density of aligned gallium phosphide (GaP) nanowires. These nanowire metamaterials, made out of an optically isotropic material, exhibit extremely large birefringence solely due to the anisotropy of the nanowire building blocks [27, 36]. The resulting birefringence is determined by the volume fraction, length and the orientation of the nanowires. Inducing form birefringence by nanostruc-

turing bulk materials represents an important approach in making III-V materials, like gallium arsenide (GaAs) and GaP, more attractive for nonlinear optics [28, 37].

A large *optical nonlinearity* as well as perfect *phase-matching conditions* are necessary in order to achieve large nonlinear yields [29]. Phase matching ensures that all the waves generated inside the nonlinear medium interfere constructively. In most materials, this phase-matching condition is not met due to material dispersion. Therefore, birefringent materials are commonly used to compensate material dispersion and phase-match the nonlinear interaction. Although bulk GaP has about 30 times larger effective second-order nonlinear susceptibility, $\chi^{(2)}_{eff}$, than that of a BBO crystal, it doesn't possess birefringence. The second harmonic (SH) signal, generated in bulk GaP, is much smaller than that of bulk BBO. The large geometrical anisotropy of aligned GaP nanowires, combined with a high refractive index contrast between the GaP and the surrounding air, gives rise to strong form birefringence and has been extensively studied by Muskens et al. [27, 36]. However, little is known about using the birefringence of these photonic metamaterials to achieve phase matching in nonlinear optical processes.

In this chapter we study second harmonic generation (SHG) in samples containing ensembles of aligned GaP nanowires randomly grown on a GaP substrate. We investigate the influence of the birefringence of the nanowire layer on second harmonic generation. We consider the symmetry of the second-order nonlinear tensor $\boldsymbol{\chi}^{(2)}$ of the nanowire metamaterials as well. The symmetry of the nonlinear tensor $\boldsymbol{\chi}^{(2)}$ of the nanowires maybe differs from that of bulk GaP due to the numerous stacking faults in the nanowires [13].

2.2 Sample description

Figures 2.1(a), (b) and (c) show cross-sectional SEM images of aligned GaP nanowires, randomly grown on a (111)B (phosphorous terminated) GaP facet. The nanowires were grown in the facilities of Philips Research. The nanowires grow preferentially along the <111>B directions and are therefore perpendicular to the surface of the substrate. The existence of a preferential growth direction can be exploited to make samples with a non-vertical orientation of the nanowires by choosing a substrate with different crystallographic orientation. For example, a (100) oriented GaP substrate can be used to grow nanowires, as shown schematically in Figure 2.2. A brief summary of the fabrication process and birefringent properties of these structures is given in this section. Additional details can be found in References [13, 27, 36].

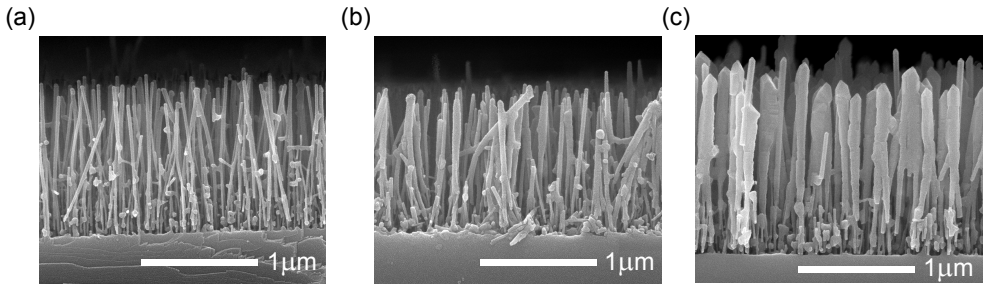

Figure 2.1. Cross-sectional SEM images of aligned GaP nanowires epitaxially grown on a (111)B GaP substrate, with a length of $\approx$ 1.3 μm and lateral shell growth times of 100 sec. (a), 350 sec. (b) and 1100 sec. (c) [38].

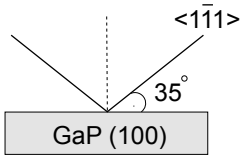

Figure 2.2. A schematic presentation of the nanowire growth on a (100) GaP substrate. Nanowires grow preferentially along the <111>B directions.

GaP nanowires are epitaxially grown using a bottom-up process of metal-organic vapor phase epitaxy (MOVPE) [13]. After depositing a 0.3 nm thick gold film on the substrate, the wafer is inserted into a MOVPE chamber and heated to a temperature of 420°C. At this temperature, the gold film breaks into $\sim$ 20 nm droplets that serve as a catalyst. Immediately after that, the precursors, tri-methyl-gallium (GaC_3H_9) and phosphine (PH_3), are introduced into the chamber and the nanowires start growing underneath the gold droplets. The length of the wires is determined by the growth time and the initial wire diameter is determined by the size of the gold droplets. The thickness of the wires can be increased by a lateral growth mechanism at an elevated temperature of 630°C. Figures 2.1(a), (b) and (c) show different wires obtained by lateral growth times of 100, 350 and 1100 seconds, resulting in volume filling fractions of nanowires f of 0.07, 0.15 and 0.4, respectively [38].

Figure 2.3 shows the experimentally determined birefringence at a wavelength of 632.8 nm (points) as a function of the nanowire volume fraction for GaP nanowires grown on a (111)B GaP substrate [27]. The birefringence in-

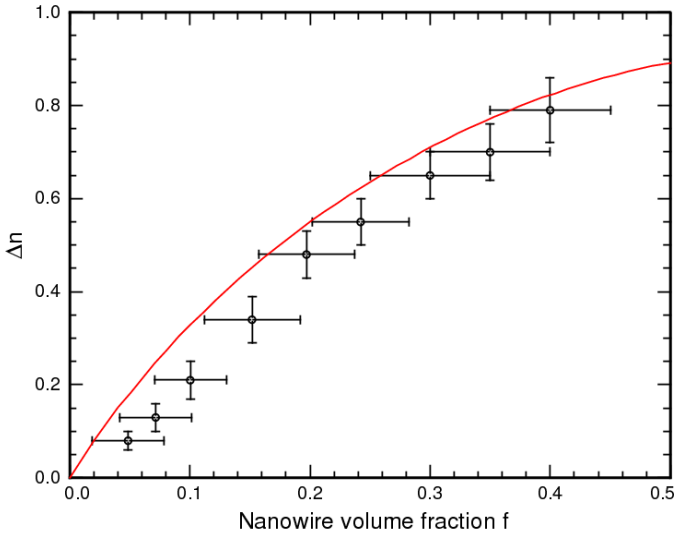

Figure 2.3. Birefringence (Δn) at a wavelength of 632.8 nm, as a function of the nanowire volume fraction (f), for GaP nanowires grown on a (111)B oriented GaP substrate. The theoretical curve (red line), calculated using Maxwell-Garnet effective medium theory, is plotted on top of the experimental data (points) taken from Ref. [27].

creases strongly with volume fraction reaching values as large as 0.79 ± 0.07 for a volume fraction of 0.4 ± 0.05.

The layer of subwavelength GaP nanowires grown on a (111)B gallium phosphide substrate can be treated as a *positive uniaxial* crystal. The birefringence $\Delta n = n_e - n_o$, with the ordinary (n_o) and the extraordinary (n_e) index of refraction, is positive, reflecting the stronger interaction with light when the **E**-field vector is parallel to the long axis of the wires. We approximate the nanowires by infinitely long cylindrical pillars, and assume that the nanowire volume fraction f is low, and use Maxwell-Garnett effective medium theory [39,40] to calculate the refractive indices n_o and n_e using the following expressions:

$$n_o^2 = \left(1 + \frac{2f\alpha}{1 - f\alpha}\right), \tag{2.1}$$

$$n_e^2 = fn^2 + (1 - f), \tag{2.2}$$

where $\alpha = (n^2 - 1)/(n^2 + 1)$ is the polarizability of cylindrical pillars, and n is the index of refraction of bulk GaP. The calculated birefringence is indicated by the red line in Fig. 2.3, and agrees very well with the experimental data.

The nanowires that we studied all have a similar length of ≈ 1.3 μm, but different samples have different volume fractions f. The wires are grown on ~ 500 μm thick (111)B oriented substrates. The relevant parameters of samples B9138 (Fig. 2.1(b)) and B9165 (Fig. 2.1(c)) are summarized in Table 2.1.

Table 2.1. Parameters of the nanowire metamaterials used in our experiments.

Sample label	GaP substrate orientation	Length (μm)	Volume fraction f (%)	Birefringence Δn
B9138	(111)B	1.26	15	0.34
B9165	(111)B	≈ 1.3	40	0.79

2.3 Setup

2.3.1 Description of the setup

Figure 2.4(a) shows a schematic of the setup used to study second harmonic generation in transmission from ensembles of aligned GaP nanowires. A Q-switched diode-pumped solid state laser (Cobolt Tango) is employed as the source of radiation at the fundamental wavelength. The laser uses an Er:Yb-doped glass as the gain medium to produce a laser beam operating in the TEM_{00} mode (M^2<1.2). The fundamental beam has a specified center wavelength of 1535 ± 1 nm and a narrow linewidth (< 0.04 nm). Short pulses, with a duration of ≈ 3.8 ns (full width at half maximum) and a ~ 1.3 kW peak power, are generated at a repetition rate of 5 kHz.

The divergent laser beam is collimated by lens L1 with a focal length of 60 mm and sent through an optical isolator (OFR IO-4-1535-HP-Z) to eliminate instability of the laser power output due to the optical feedback. During the measurements, we check for laser power fluctuations by monitoring the output of the internal laser photodiode using a Lab View program.

The combination of a half-wave ($\lambda/2$) plate and a Glan-Thompson polarizing beamsplitter cube (POLARIZER) is used to define the polarization and can be used to attenuate the power of the incident fundamental beam if desired. The fundamental beam is focused onto the sample by lens L2 with a focal length of 175 mm, and the generated second harmonic is collected and collimated in transmission by lens L3 (focal length of 175 mm). We can set the angle of incidence θ, the azimuthal angle φ, and the position of the sample

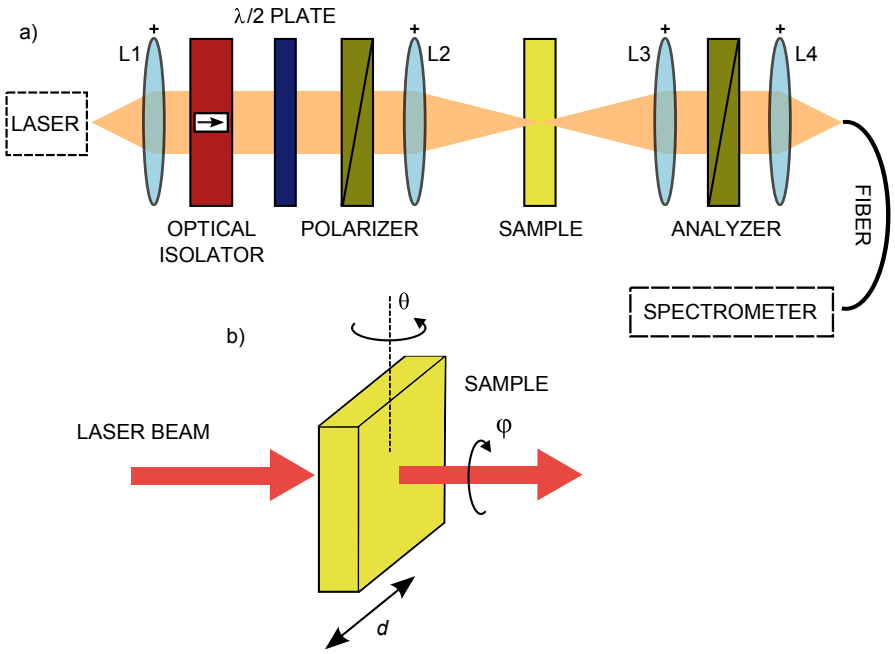

Figure 2.4. (a) Setup used for investigating the second harmonic generation in transmission from nanowire metamaterials. The fundamental beam is focused on the sample and the generated second harmonic is collected in transmission and forwarded to a fiber-coupled spectrometer. Lenses L1–L4 serve to focus and collimate the light. The polarization of the incident fundamental is defined using a combination of a $\lambda/2$ plate and a polarizer. The polarization state of the second harmonic is studied with a second polarizer (analyzer). An optical isolator is employed to prevent optical feedback caused by the light reflecting back into the laser cavity. (b) Details of the sample stage. The angle of incidence θ, the azimuthal angle φ, and the position of the sample d, can be set individually using motorized stages.

d, individually, using motorized stages, as sketched in Figure 2.4(b). A second Glan-Thompson polarizing beamsplitter cube (ANALYZER) is used to study the polarization properties of the SH light. In the end, the second harmonic is focused by lens L4 (focal length of 15.3 mm) onto a 600 μm multimode fiber and sent to a fiber-coupled grating spectrometer USB4000 (resolution $\approx$ 1.3 nm).

2.3.2 Second harmonic generation from BBO

In order to test the setup and our 1535 nm laser we generated second harmonic using a 1 mm BBO crystal. Figure 2.5 shows the measured second harmonic signal as a function of angle of incidence (black dots). The phase matching in this standard crystal is well-known. For a collinear second harmonic generation the power at the SH frequency $P(2\nu)$ is proportional to the square of the power at the fundamental frequency $P(\nu)$, and can be expressed as [29]:

$$P(2\nu) \propto L^2 \mathrm{sinc}^2\left(\Delta k L/2\right) P(\nu)^2, \tag{2.3}$$

where

$$\mathrm{sinc}^2\left(\Delta k L/2\right) = \frac{\sin^2\left(\Delta k L/2\right)}{\left(\Delta k L/2\right)^2}, \tag{2.4}$$

and

$$\Delta k = 2k(\nu) - k(2\nu) = \frac{4\pi\nu}{c}\left(n(\nu) - n(2\nu)\right). \tag{2.5}$$

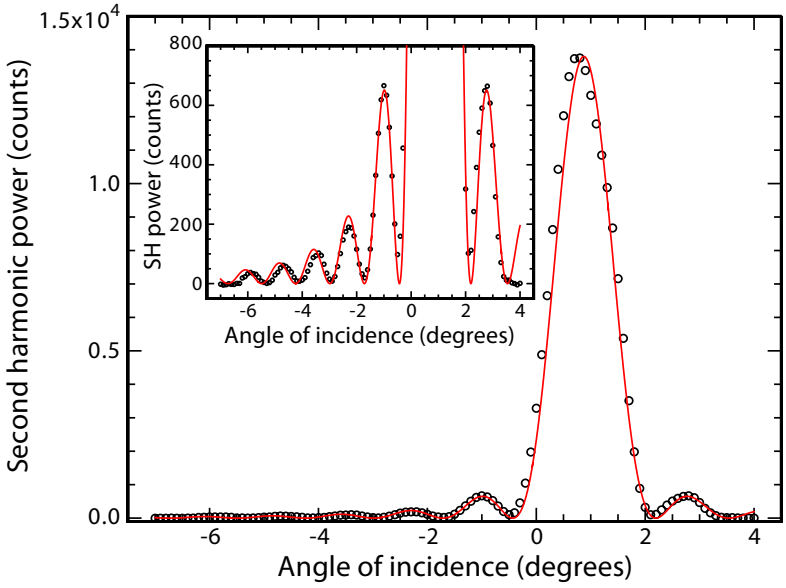

Figure 2.5. Second harmonic power as a function of angle of incidence (black dots), generated in a 1 mm BBO crystal, and measured in transmission. The red line is a fit obtained by considering the phase-matching condition in a negative uniaxial crystal (see text). The SH signal reaches maximum when the phase-matching condition is satisfied. The inset zooms in on lower values of SH power emphasizing the good agreement of higher order maxima.

Here $k(\nu)$ and $k(2\nu)$ are the wave vectors at the fundamental and the second harmonic frequency, respectively. Thickness of the crystal is denoted by L. When the refractive index at the fundamental frequency ($n(\nu)$) is equal to the refractive index at the SH frequency ($n(2\nu)$), $\Delta k = 0$ and the phase-matching condition is satisfied resulting in maximum SH yield. For a BBO crystal, phase matching can be achieved by choosing the polarization of the SH wave to be extraordinary so that it experiences the lower of the two refractive indices. We employ type II phase matching where one of the waves at the fundamental frequency is an extraordinary wave while the other wave is an ordinary wave. The phase-matching condition $\Delta k = 0$ can then be expressed as:

$$n_o(\nu) + n_e(\nu, \psi) - 2n_e(2\nu, \psi) = 0, \tag{2.6}$$

where ψ is the angle between the wave vector $\mathbf{k}$ and the optic axis of the BBO crystal. The refractive index $n_e(\nu, \psi)$ is given by

$$\frac{1}{n_e(\nu, \psi)^2} = \frac{\sin^2 \psi}{n_e(\nu, 90°)^2} + \frac{\cos^2 \psi}{n_o(\nu)^2}. \tag{2.7}$$

In the experiment, the fundamental beam is polarized under an angle of 45° with respect to the plane containing the wave vector $\mathbf{k}$ of the incident light and the optic axis. The crystal is cut so that the type II phase-matching condition is satisfied close to normal incidence. The fundamental beam is focused to a spot of ≈ 120 μm with a numerical aperture (NA) ≈ 0.01, and the angle of incidence θ is varied from -7° to 4° in steps of 0.1°. By varying the angle of incidence θ we vary the angle ψ between the wave vector $\mathbf{k}$ and the optic axis.

To fit the experimental data, we use Equation 2.3 with $A = L^2 P(\nu)^2$ as a fitting parameter. The phase mismatch Δk is given by the known refractive indices of BBO:

$$\Delta k = \frac{2\pi\nu}{c} \left(n_o(\nu) + n_e(\nu, \psi) - 2n_e(2\nu, \psi) \right). \tag{2.8}$$

Here ψ is the angle between the wave vector $\mathbf{k}$ and the optic axis inside the material. We use an additional fitting parameter which describes the angle between the optic axis and the surface normal. As can be seen from Figure 2.5, the obtained fit (red solid line), agrees well with the experimental data. The inset shows that even the secondary maxima of the sinc^2 function are nicely reproduced.

2.4 SHG in samples with GaP nanowires

Figure 2.6 shows the measured power of the signal at a frequency of 390.9 THz (wavelength of 767.5 nm) as a function of the power of the incident fundamental beam (black dots), generated in transmission from sample B9165. The inset shows a typical spectrum of the signal detected by a fiber-coupled spectrometer USB4000. We focus the fundamental beam to a spot of ≈ 120 μm with a numerical aperture ≈ 0.01, and keep the angle of incidence as well as the polarization of the incident fundamental constant throughout the measurement. The power at the second harmonic frequency grows with the square of the fundamental power, as indicated in Fig. 2.6 with a linear fit (red line) of a slope of 1.975±0.008.

The crucial question is whether this second harmonic signal is generated in the nanowire layer or in the underlying substrate. One possibility is to use the birefringence of the nanowires to achieve phase matching via angle tuning of

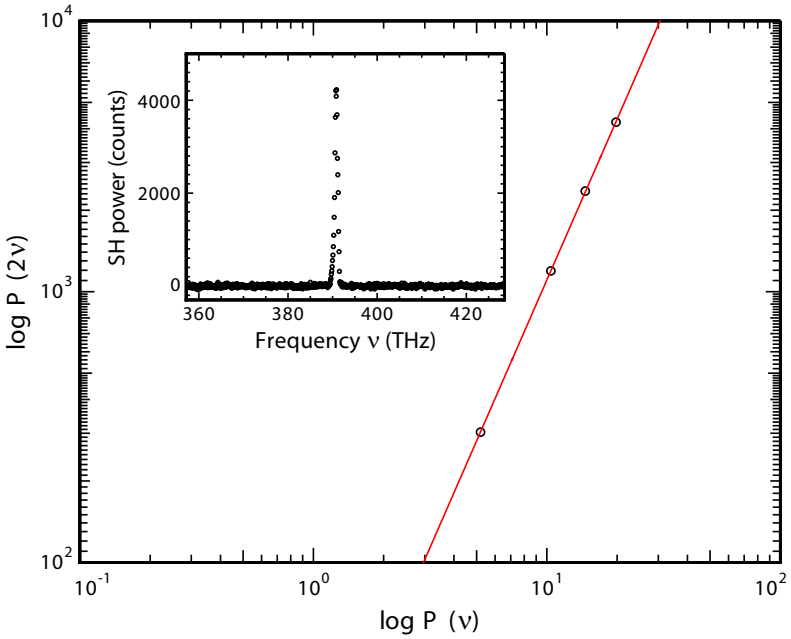

Figure 2.6. Measured power of the signal at a frequency of 390.9 THz (wavelength of 767.5 nm) as a function of the fundamental power (black dots), generated in transmission from sample B9165. The red line represents a linear fit confirming the quadratic power dependence. A typical spectrum of the SH signal is shown in the inset.

the sample. When successful, a much more efficient SHG would be obtained from the nanowire layer than from the substrate. Unfortunately, it is not possible to demonstrate this with short nanowires with a length of ≈ 1.3 μm, which is smaller than the coherence length L_c. This coherence length is defined as $L_c = 2/\Delta k$ [29], where Δk is given by Equation 2.5, and defines a length over which the fundamental and second harmonic waves are in phase. For a bulk GaP crystal used for frequency doubling of 1535 nm light, the coherence length L_c is about 3 μm. The large value of Δk for bulk GaP is due to the strong dispersion of the material. For a nanowire layer that contains mostly air, the effective refractive index and consequently also the dispersion are lower than that of the bulk. Therefore, we expect a smaller Δk and thus a longer coherence length. Phase matching which reduces Δk and increases L_c is only effective if the crystal thickness L is much larger than L_c ($L >> L_c$). To enhance the second harmonic signal due to the nanowires by phase matching, we could make the nanowires much longer than the coherence length. However, long nanowires (> 10 μm) have a significantly reduced birefringence due to the bending of the wires [27]. Therefore, a sample with these long nanowires is not a good candidate for efficient second harmonic generation.

In the remainder of the chapter we will discuss two possibilities to find out whether the measured second harmonic signal in Figure 2.6 is generated in the nanowire layer or in the underlying substrate. In Section 2.4.1 we discuss a possible difference in tensor properties of $\boldsymbol{\chi}^{(2)}$ between the bulk material and the nanowires. In Section 2.4.2 we discuss an experiment where we use the strong absorption of blue light in GaP to get rid of the substrate contribution.

2.4.1 Tensor properties of nanowires

Figures 2.7(a) and (b) show polar plots of the measured SH signal in transmission as a function of the azimuthal angle φ for sample B9165 and a (111) oriented GaP reference substrate, respectively. The experimental data are offset by 500 counts for clarity. The fundamental beam is at normal incidence, and is focused to a spot of ≈ 120 μm with a numerical aperture ≈ 0.01. The azimuthal angle φ (Fig. 2.4(b)) is varied from 0° to 360° in steps of 3°. The black dots and red triangles in Figure 2.7 correspond to the experimental data points for the parallel and the orthogonal orientation of the polarizer and the analyzer. In this way we probe some of the symmetry properties of the nonlinear susceptibility tensor $\boldsymbol{\chi}^{(2)}$.

Bulk gallium phosphide crystalizes in zincblende structure, which has point group $\bar{4}3m$ symmetry. The crystal structure of the nanowires is also predominantly zincblende, as determined by high resolution transmission electron

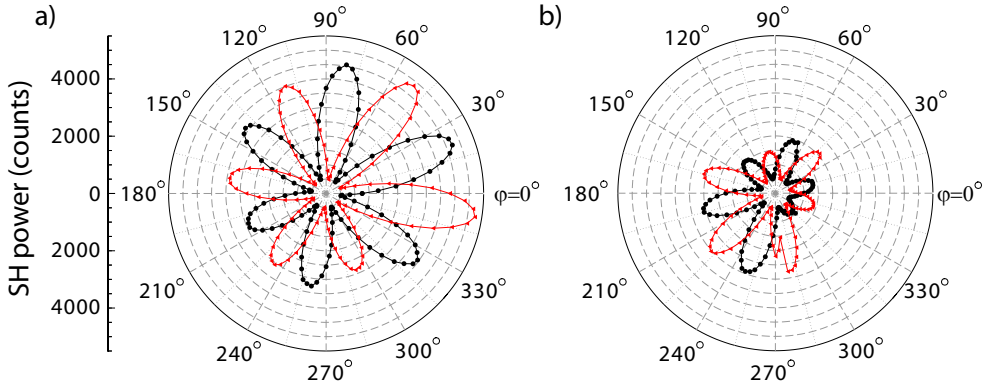

Figure 2.7. Measured SH power as a function of the azimuthal angle φ for (a) sample B9165 and (b) a (111) oriented GaP reference substrate, offset by 500 counts for clarity. The SH signal is measured in transmission at normal incidence. Black dots (red triangles) correspond to experimental data points for the parallel (orthogonal) orientation of the polarizer and the analyzer (Fig. 2.4(a)). Solid lines serve only as a guide to the eye. As expected, the power at the SH frequency is proportional to $\sin^2(3\varphi)$ ($\cos^2(3\varphi)$).

microscopy (HRTEM) [36]. At the same time, the crystal structure of the nanowires contains many stacking faults [13]. To understand the nature of these defects let us consider the stacking sequence of atomic layers in a cubic zincblende structure [12]. In a perfect zincblende structure the atomic layers are stacked in an ...ABCABC... (fcc) sequence along the [111] direction. A stacking fault of the hexagonal layers locally changes the stacking sequence to ...ABAB... (hcp), and as a result a hexagonal wurtzite crystal structure is formed. For GaP nanowires that grow along a [111] direction of the cubic lattice, the wurtzite domains are oriented along a [0001] direction of the hexagonal lattice [12]. The wurtzite structure belongs to a $6mm$ point group symmetry, and has a different second-order nonlinear susceptibility tensor compared to a zincblende structure. To appreciate the difference we use a contracted notation for the nonlinear susceptibility tensor. Instead of the rank 3 tensor $\boldsymbol{\chi}^{(2)}$ we use a 6×3 rank 2 tensor $\boldsymbol{d}$ with elements d_{ij} [29]. For zincblende (group $\bar{4}3m$) the elements d_{14}, d_{25}, and d_{36} are all equal and nonzero. For wurtzite (group $6mm$) the nonzero elements are $d_{15} = d_{24}$, $d_{31} = d_{32}$, and d_{33}.

Let's calculate the SH power as a function of the azimuthal angle φ, generated in transmission from a (111) oriented GaP slab, at normal incidence of

the fundamental beam. Instead investigating a system in which the sample is rotated, we study an equivalent problem where both the incident polarization of the fundamental and the analyzer are rotated by the same angle φ while the sample is fixed.

The nonlinear polarization $\mathbf{P}^{NL}(2\nu)$ generated by the electric field $\mathbf{E}(\nu)$ in the medium is given by [29]

$$\mathbf{P}^{NL}(2\nu) = 4d_{14} \begin{pmatrix} E_y(\nu)E_z(\nu) \\ E_x(\nu)E_z(\nu) \\ E_x(\nu)E_y(\nu) \end{pmatrix}, \tag{2.9}$$

where $E_x(\nu)$, $E_y(\nu)$, and $E_z(\nu)$ are the electric field components along the x, y, and z-axis of the Cartesian coordinate system, respectively. Here, we define x, y, and z-axis to coincide with the crystallographic axes [100], [010], and [001].

We chose unit vectors $\frac{1}{\sqrt{2}}(1,-1,0)$, $\frac{1}{\sqrt{6}}(1,1,-2)$, and $\frac{1}{\sqrt{3}}(1,1,1)$, denoted by $\mathbf{e}_1$, $\mathbf{e}_2$, and $\mathbf{e}_3$, respectively, to form an orthonormal basis of $\mathbf{R}^3$. At normal incidence, the wave vector $\mathbf{k}$ of the incident fundamental is parallel to $\mathbf{e}_3$ with the $\mathbf{E}$-field in the plane spanned by $\mathbf{e}_1$ and $\mathbf{e}_2$. Consequently, the incident electric field $\mathbf{E}(\mathbf{r},t)$ as a function of the azimuthal angle φ is given by

$$\mathbf{E}(\mathbf{r},t) = \mathbf{E}(\nu,\varphi)e^{-i2\pi\nu t} + \mathbf{E}(-\nu,\varphi)e^{+i2\pi\nu t}, \tag{2.10}$$

where

$$\begin{aligned} \mathbf{E}(\nu,\varphi) &= \frac{1}{2}E_0 e^{i\mathbf{kr}} \left(\cos(\varphi)\mathbf{e}_1 + \sin(\varphi)\mathbf{e}_2\right) \\ &= \frac{1}{2}E_0 e^{i\mathbf{kr}} \begin{pmatrix} \frac{\cos(\varphi)}{\sqrt{2}} + \frac{\sin(\varphi)}{\sqrt{6}} \\ \frac{\sin(\varphi)}{\sqrt{6}} - \frac{\cos(\varphi)}{\sqrt{2}} \\ -\sqrt{\frac{2}{3}}\sin(\varphi) \end{pmatrix}. \end{aligned} \tag{2.11}$$

Here, $\mathbf{E}(-\nu,\varphi)$ is the complex conjugate of $\mathbf{E}(\nu,\varphi)$, and E_0 is the amplitude of the electric field. Combining Equations 2.9 and 2.11, we arrive to the following expression for the Cartesian components of the nonlinear polarization $\mathbf{P}^{NL}(2\nu)$ as a function of the azimuthal angle φ:

$$\begin{aligned} P_x^{NL}(2\nu,\varphi) &= \tfrac{2}{3}E_0^2 d_{14}\sin(\varphi)\left(\sqrt{3}\cos(\varphi) - \sin(\varphi)\right), \\ P_y^{NL}(2\nu,\varphi) &= -\tfrac{2}{3}E_0^2 d_{14}\sin(\varphi)\left(\sqrt{3}\cos(\varphi) + \sin(\varphi)\right), \\ P_z^{NL}(2\nu,\varphi) &= -\tfrac{1}{3}E_0^2 d_{14}\left(1 + 2\cos(2\varphi)\right). \end{aligned} \tag{2.12}$$

The measurement scheme with the parallel (orthogonal) orientation of the polarization of the incident fundamental and the analyzer, filters through the nonlinear polarization $P_{\parallel}^{NL}(2\nu,\varphi)$ ($P_{\perp}^{NL}(2\nu,\varphi)$), given by

$$\begin{aligned} P_{\parallel}^{NL}(2\nu,\varphi) &= \mathbf{P}^{NL}(2\nu)\,(\cos(\varphi)\mathbf{e}_1+\sin(\varphi)\mathbf{e}_2) \\ &= -\sqrt{\frac{2}{3}}E_0^2 d_{14}\cos(3\varphi), \qquad (2.13) \\ P_{\perp}^{NL}(2\nu,\varphi) &= \mathbf{P}^{NL}(2\nu)\,(\sin(\varphi)\mathbf{e}_1-\cos(\varphi)\mathbf{e}_2) \\ &= \sqrt{\frac{2}{3}}E_0^2 d_{14}\sin(3\varphi). \qquad (2.14) \end{aligned}$$

The corresponding expressions for the SH power as a function of the azimuthal angle φ, $P_{\parallel}(2\nu,\varphi)$ and $P_{\perp}(2\nu,\varphi)$, are proportional to the square of the nonlinear polarizations $P_{\parallel}^{NL}(2\nu,\varphi)$ and $P_{\perp}^{NL}(2\nu,\varphi)$, respectively:

$$P_{\parallel}(2\nu,\varphi) \propto \cos^2(3\varphi), \qquad (2.15)$$

$$P_{\perp}(2\nu,\varphi) \propto \sin^2(3\varphi). \qquad (2.16)$$

As can be seen from Fig. 2.7, the experimentally obtained SH signal qualitatively exhibits the $\sin^2(3\varphi)$ ($\cos^2(3\varphi)$) dependence, for both the reference (111) GaP substrate and sample B9165. We observe six lobes in the polar plots and the fact that all the minima really go to zero, once the offset of 500 counts is subtracted. However, the amplitudes of the lobes vary, probably due to a non-perfect alignment. Namely, the wave vector $\mathbf{k}$ of the incident fundamental does not exactly coincide with the rotation axis of the sample. As a result, the fundamental beam describes a circle on the sample during the measurement. Most probably, the SH signal fluctuates from spot to spot on the sample due to the variation in the sample thickness. These fluctuations of the second harmonic signal are essentially *Maker fringes* [41].

With currently available samples, one might be tempted to employ an experimental scheme where the wave vector $\mathbf{k}$ of the fundamental beam is perpendicular to a (100) substrate from which the nanowires grow preferentially in the <111>B directions (Fig. 2.2). If a Cartesian coordinate system with a z-axis parallel to the vector $\mathbf{k}$ is adopted, the only component of the nonlinear polarization that can be generated in the substrate is $P_z^{NL}(2\nu)$, and this cannot give rise to a SH signal in transmission. Let's consider now a single pair of nanowires that form a V-shaped structure in the <111>B directions (Fig. 2.2) on top of the substrate. In principle, the symmetry of the $\boldsymbol{\chi}^{(2)}$ tensor is such that a SH signal can be generated in transmission from the

wurtzite domains in a single nanowire. However, due to a geometric symmetry of the V shape, the components of the nonlinear polarization perpendicular to the wave vector $\mathbf{k}$ of the fundamental, generated in the two nanowires, cancel each other. Thus, there is no SH signal generated in transmission from the nanowires either.

2.4.2 Second harmonic generation at 425 nm

Figure 2.8 shows the SH signal at a wavelength of 425 nm as a function of the position of the fundamental beam on the sample (black dots), measured in transmission for sample B9138 with a 15% volume fraction of nanowires. The fundamental beam at a wavelength of 850 nm enters the sample at normal incidence from the substrate side (see inset) generating second harmonic as it propagates. Since the absorption length at a wavelength of 425 nm is only $\sim$ 200 nm for bulk GaP, we can assume that the SH signal in transmission is due to a thin layer (< 1 μm) of the side of the sample facing the detector.

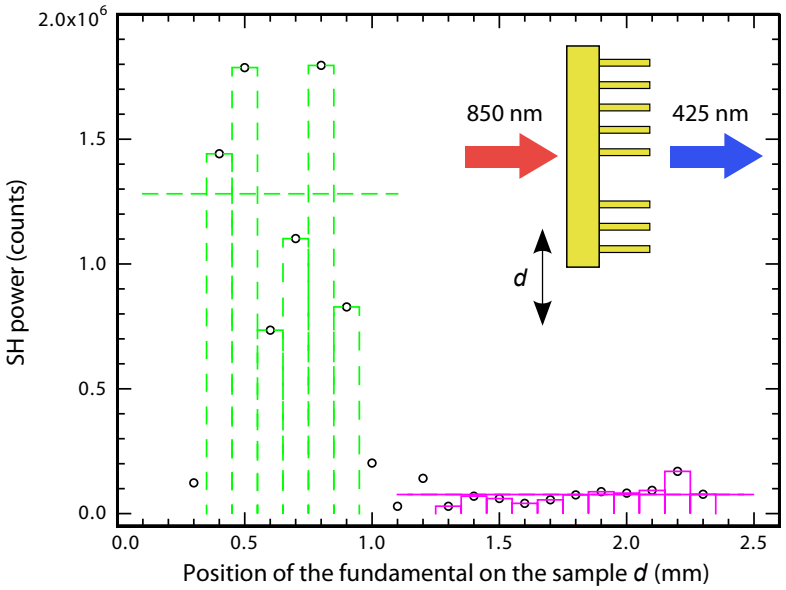

Figure 2.8. Measured SH signal in transmission as a function of the position of the fundamental beam on sample B9138. A scheme of the experimental geometry is presented in the inset. The dashed (solid) bars indicate the signal generated from a region without (with) the nanowires. The horizontal dashed (solid) line indicates the average SH signal.

Therefore, for the fundamental beam exiting the sample through the nanowire layer, the SH signal should have a large component due to the nanowires. By translating the sample relative to the fundamental beam we probe regions with and without the nanowires, without changing the angle of incidence on the sample.

In the experiment, the setup from Fig. 2.4(a) is slightly modified. A Ti:Sapphire laser is used to generate pulses at 850 nm with a duration of $\sim$ 2 ps full width at half maximum at a repetition rate of 80 MHz. The fundamental is focused to a spot of $\sim$ 30 μm by a lens with a focal length of 100 mm. Since the nanowire layer acts as a highly scattering medium for radiation at 425 nm [36], a lens with a high NA of 0.5 and a focal length of 8 mm is used to collect the SH signal in transmission. The collimated second harmonic is focused onto a Peltier cooled CCD. A combination of the Newport bandpass filter FSR-BG39, with a transmission region of $\approx$ 350–600 nm, and the Thorlabs shortpass filter FES0550, with a cut-on wavelength of about 550 nm, is inserted before the CCD to filter out the fundamental beam, and ensure the detection of the second harmonic signal only.

The dashed and solid bars in Figure 2.8 correspond to the SH signal originating from the region without and with nanowires, respectively. The average second harmonic signal generated in the region without nanowires (horizontal dashed line) is $\approx$ 17 times larger than the average second harmonic signal generated in the region with nanowires (horizontal solid line). Apparently, nanowires on the sample do not lead to enhanced second harmonic generation in the forward direction. We speculate that the main contribution of the nanowires is to scatter the second harmonic generated in bulk GaP to angles inside the high refractive index substrate. This scattered second harmonic signal is not collected by our setup. Unfortunately, the current experimental data do not distinguish between scattered light and light generated by the nanowires, preventing a more detailed quantitative analysis.

2.5 Conclusion

The coherence length for second harmonic generation in bulk GaP at a wavelength of 1535 nm is more than two times larger then the wire length of short GaP nanowires with a length of $\approx$ 1.3 μm. As a result, the contribution to the SH signal originating from the substrate is likely to be larger than the contribution originating from the nanowire layer.

In order to separate and identify the second harmonic due to the nanowires, we tried to eliminate the substrate contribution to the SH signal by exploring

the symmetry of the nonlinear tensor $\boldsymbol{\chi}^{(2)}$, and by an experiment at a second harmonic wavelength of 425 nm at which GaP is highly absorbing. Stacking faults in the nanowires lead to a locally different crystal structure (wurtzite) compared to bulk GaP (zincblende). With currently available samples, we were unable to define an appropriate experimental geometry to exploit this symmetry and generate signal from nanowires only. For second harmonic generation at an absorbing wavelength, the obtained experimental data can be explained by SH generated in the substrate and scattered by the nanowires.

Replacing the GaP substrate with another substrate that has a very low, if not zero, second-order nonlinear susceptibility, while maintaining the original orientation of the nanowires, is probably the best way to study the second harmonic generation in ensembles of aligned nanowires [42].